Effect of thermal annealing on electrical and photoelectrical properties of *n*-InSb

S.V. Stariy, A.V. Sukach, V.V. Tetyorkin, V.O. Yukhymchuk, T.R. Stara
V. Lashkaryov Institute of Semiconductor Physics, NAS of Ukraine, Ukraine
Phone (38 044) 525-54-61, e-mail: teterkin@isp.kiev.ua

Abstract. InSb wafers of *n*-type conductivity were annealed at 300, 370 and 400 °C for 30 min in an open tube system under flowing argon ambient. The conductivity type conversion are revealed for the first time in samples with the electron concentration ~$1.0 \cdot 10^{14}$ cm^{-3} for all annealing temperatures. Experimental evidences have been obtained that this phenomenon has a bulk character. In annealed samples the spectral response exhibits pronounced increase in the short-wave region. The effect of annealing on electrical and photoelectrical properties of *n*-InSb has been explained by formation of In$_{Sb}$ antisites.

Keywords: InSb, thermal annealing, conductivity type conversion, native defects, indium antisites.

1. Introduction

In semiconductor technology, initial wafers of semiconductor material are usually doped by diffusion or ion implantation of impurity atoms. The doped semiconductors are subjected to thermal annealing to reduce a number of diffusion or implantation damages, as well as to activate implanted ions. The conventional long-term furnace annealing and rapid thermal annealing (RTA) processes are used for this purpose. Both processes have their own advantages and disadvantages. For instance, the furnace annealing results in dopant profile broadening as well as evaporation of volatile component in $A^{III}B^V$ and $A^{II}B^{IV}$ semiconductors. To suppress the loss of volatile components, capsulation layers are usually deposited onto the surface of samples. The RTA seems to be more suitable for the processing of implanted semiconductors, because it offers the advantage of fast removing the implantation damages together with the less dopant profile broadening. At the

same time, there are indications that the implanted $A^{III}B^V$ materials suffer from defects generated during RTA [1]. As to InSb, it has been pointed out that the stoichiometry of InSb in the surface region can be destroyed by any annealing treatment at temperatures exceeding 350 °C [2]. The RTA of Be implanted wafers at temperatures higher than 350 °C show deficiency of Sb in the subsurface layer [3]. Taking into account the discrepant data on the annealing processes in InSb, the aim of this work was to study the effect of furnace annealing on electrical and photoelectrical properties of InSb wafers as well as to clarify the nature of defects generated by the annealing.

2. Experimental details

The samples for electrical and photoelectrical measurements were cut from InSb (111) wafers of *n*-type conductivity with the thickness close to 500 μm. The etch pits density in the wafers was less than 10^2 cm^{-2}. An

open tube system was used for the annealing of InSb wafers in a flowing argon atmosphere at the temperatures 300, 370 and 400 °C for 30 min. No capsulation layers were deposited onto the surface of samples. Electrical parameters of samples were obtained from the Hall effect and specific resistance measurements in the magnetic field 0.3 kOe. The electron concentration in the reference samples was close to $1.0 \cdot 10^{14}$ cm^{-3} at 77 K. The photoconductivity response and photoelectromagnetic effect (PEM) measurements were carried out using the standard technique with low-frequency modulation of radiation. A weak signal condition δn, $\delta p << n$, p was fulfilled, where δn and δp are the concentration of non-equilibrium electrons and holes. The surfaces of samples were mechanically polished and chemically etched directly before measurements. The spectral distribution of infrared radiation source (Globar) was determined using a calibrated pyroelectric sensor. The photocurrent spectra were measured in samples of p-type conductivity doped for comparison.

3. Experimental results and discussion

The most important result of the furnace annealing is the conductivity type conversion from an n-type to a p-type observed at all annealing temperatures. Typical temperature dependences of carrier concentration in the reference (unannealed) and annealed samples are shown in Fig. 1. As seen, in the annealed samples the hole concentration increases with the annealing temperature increase from 300 up to 370 °C and remains practically unchanged at higher annealing temperatures. The hole mobility exhibits slight increase in the whole range of annealing temperatures, but its magnitude is several times lower in comparison with the values published in the literature [4] for p-type materials of high quality (Fig. 2).

Fig. 3 shows the photocurrent spectra measured at 77 K. In the reference sample, the spectrum has the typical shape for InSb single crystals, namely: the photocurrent rises rapidly in the long-wave region, reaches a peak value at the wavelengths $\lambda_p \approx$ 5.3…5.4 µm and saturates in the short-wave region. Note that the peak wavelength λ_p exceeds the wavelength value $\lambda_g = hc/E_g$, which corresponds to the energy gap E_g. The photocurrent saturates at the short wavelengths with the magnitude that depends on the surface treatment. For comparison, experimental measurements were carried out for the surfaces etched in CP4A and HBr+Br$_2$ solutions (Fig. 3, curves 1 and 2, respectively). By fitting the calculated and experimental data, the surface recombination velocity of $7 \cdot 10^3$ and $1.4 \cdot 10^4$ cm/s was estimated for CP4A and HBr+Br$_2$ solutions, accordingly. Similar values were obtained earlier for InSb of n-type conductivity [4]. The details of the photocurrent calculation in n-InSb are given in Appendix. The important result was obtained for the annealed sample of p-type conductivity (Fig. 4, curve 3).

As seen, in contrast with the reference sample the photocurrent exhibited a marked increase in the short-wave region. Note that this dependence was observed in the annealed sample only. In the samples of p-type conductivity doped in a conventional manner, photo-current spectra had a shape similar to that shown in Fig. 3 for n-InSb.
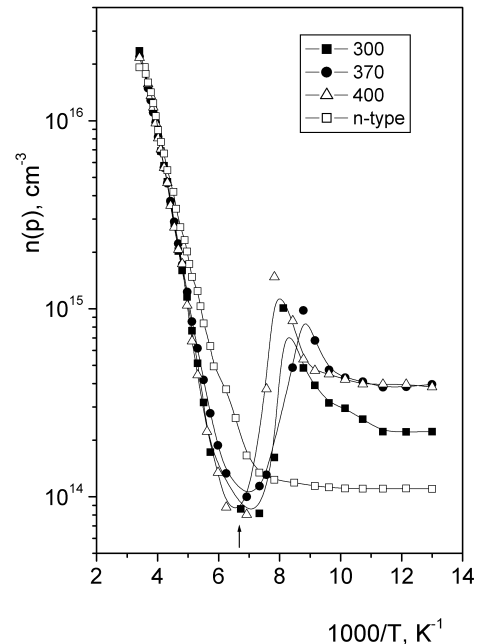
Fig. 1. Temperature dependences of electron and hole concentration in the reference sample of n-type conductivity (*1*) and annealed samples (*2-4*) of p-type conductivity. The arrow marks the temperature of p-to-n transition.
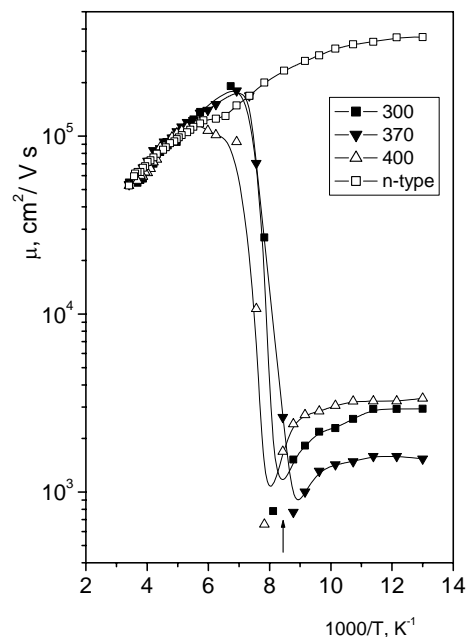
Fig. 2. Carrier mobility vs temperature in the reference and annealed samples. The designations are the same as in Fig. 1.
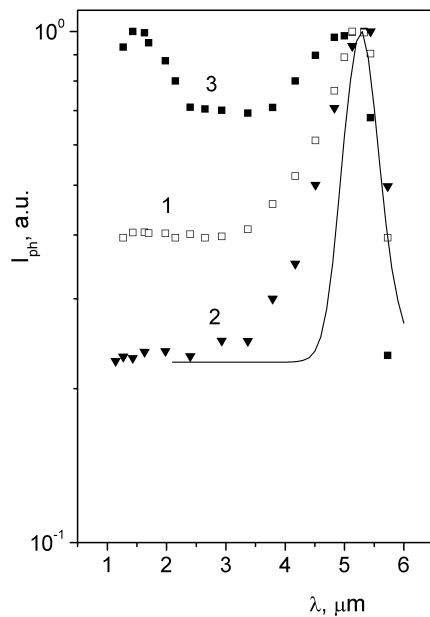
Fig. 3. Photocurrent per incident photon spectra in the reference (*1*, *2*) and annealed at 300 °C (*3*) samples measured at 77 K. The solid line represents the calculated spectrum. The surface is etched in CP4A (*1*, *3*) and HBr+Br$_2$ (*3*) solutions.

In Fig. 4, the field dependences of PEM in InSb samples of *n*- and *p*-type conductivities are shown. Surface of the samples was etched in CP4A solution. In the reference sample of *n*-InSb, PEM linearly depends on the magnetic field *B* up to 12 kOe. Due to low mobility of minority carriers (holes), the condition of strong magnetic field $\mu_p H/c > 1$ is not reached in this case. By contrast, in the annealed sample of *p*-type conductivity the field dependence of current $I_{PME}(H)$ deviates from linearity at a relatively low magnetic field ($H = 1.5$ kOe), indicating that the condition $\mu_n H/c \gg 1$ is reached for electrons. From the slope of $I_{PME}(H)$ dependence, the electron mobility value was estimated to be $8 \cdot 10^4$ cm^2/V·s at 77 K.

In relation with the experimental data, several remarks should be made. The conductivity type conversion seems to be a bulk phenomenon. At least, this conclusion was made for the investigated sample annealed at the lowest temperature. To prove it, the sheet resistance and thermoEMF was repeatedly measured in the sample thinned by chemical etching up to the thickness of ~100 μm. Obviously, there is no doubt that this conclusion remains valid for higher annealing temperatures. To interpret experimental data correctly, there is a need to consider the nature as well as evolution of native defects caused by thermal treatment. Unfortunately, there are very few experimental studies of native defects in bulk crystals and epilayers of InSb [5-8]. At the same time, comprehensive theoretical investigations were recently published in the literature [9-11]. However, when comparing theoretical and experimental data, difficulties arise due to the fact that theoretical calculations were made for the thermal equilibrium conditions, which cannot be entirely realized in the annealing process. Thus, it is difficult to predict a particular type of defects that can be realized in an annealing process. In further analysis, experimental data and theoretical models developed for the annealed GaAs were also taken into account [12-14].

Since the investigated samples were not encapsulated, the surface decomposition and preferential evaporation of volatile component (Sb) from the surface can occur [15]. Experimentally, in the investigated samples an excess Sb at the surface has been detected by Raman scattering measurements. Fig. 5 shows the room temperature Raman spectra measured in the reference and annealed samples. To prevent their heating during measurements, the low-intensity laser excitation at the wavelength 532 nm was used. As seen, in the initial sample the spectrum consists of the bulk TO and LO peaks at 178 and 187 cm^{-1}, respectively, whereas in the annealed samples two additional peaks at 115.5 and 155 cm^{-1} arose. These peaks can be attributed to E_g and A_{1g} modes of crystalline Sb [15].

Obviously, evaporation and segregation of Sb at the surface results in formation of vacancies at the anion sub-lattice. Beside vacancies, the most important native point defects in A$_3$B$_5$ semiconductors are interstitials, antisites and antisite pairs. The formation energies, densities, atomic and electronic structures of grown-in defects were theoretically analyzed in bulk crystals under thermal equilibrium condition [9-11]. Different charge states of these defects were modeled as a function of the Fermi level. So, the impact of different growth conditions on the formation energies was taken into account. In InSb, possible acceptor defects are In$_{Sb}$ antisites and In vacancies. Generally, In$_{Sb}$ antisites can be neutral, singly and doubly negatively charged defects [11]. Accordingly, Sb$_{In}$ antisites can be neutral, singly and doubly negatively charged ones. However, the small band gap of InSb limits formation of many charged defects. Thus, only the neutral and −1 charge states for In$_{Sb}$ and the +1 and neutral charge states for Sb$_{In}$ are possible [11]. Sb$_{In}$ antisites are more stable than the In$_{Sb}$ ones under Sb-rich condition, whereas under In-rich condition In$_{Sb}$ antisites are favored over Sb$_{In}$. Due to the difference in formation energies between the two antisites is not large, both defects should be observed. The antisite pairs In$_{Sb}$-Sb$_{In}$ are assumed to be neutral [11]. The formation energies for In$_{Sb}$ and Sb$_{In}$ antisites under stoichiometric condition are estimated to be 1.46 and 1.29 eV, respectively [11]. The formation energies of In and Sb vacancies for the same condition are 2.57 and 1.69 eV, accordingly [10]. Large difference between the energies implies that antisite defects dominate over vacancies under stoichiometric conditions, when the Fermi level is $E_g/2$. However, under different growth and doping conditions, vacancy energies can be lower than those for antisites, and the dominant intrinsic defect type may change.
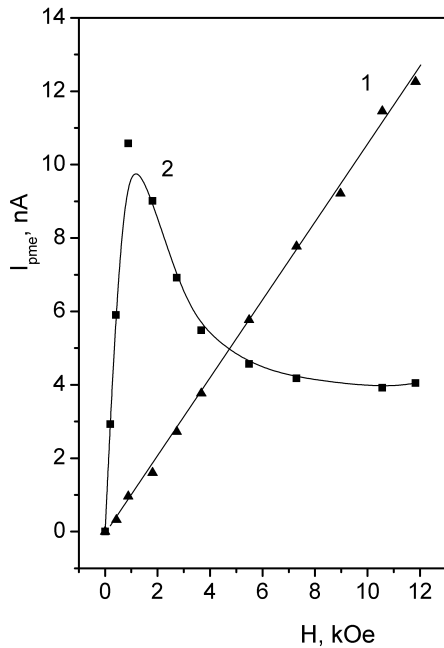
Fig. 4. Field dependences of photoelectromagnetic effect in the reference (*1*) and annealed at 300 °C (*2*) samples measured at 77 K.
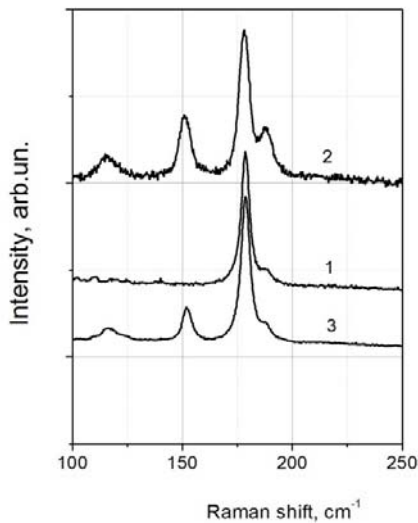
Fig. 5. Room temperature Raman spectra in the reference (*1*) and annealed at 300 and 400 °C samples (curves *2* and *3*, respectively).

The *p*-type conversion called the thermal conversion in GaAs subjected to RTA or furnace annealing is known for many years [12-14]. Several models of this phenomenon have been proposed in literature, but today the most reasonable one is formation of Ga_{As} antisites [12-14]. It is clear from the above analysis that Sb vacancies cannot be responsible for conductivity type conversion due to their donor-like nature. Similarly to that in GaAs, it can be assumed that In_{Sb} antisites are mainly responsible for this phenomenon

in the annealed InSb. Together with In vacancies and residual acceptors, they determine the hole concentration in the annealed samples. If this assumption is true, it means that Sb vacancies are not stable with respect to formation of In_{Sb} antisites. Since the energy states of In_{Sb} antisites are not known, the hole concentration at 77 K in the annealed samples may be regarded as a lower limit for the density of In_{Sb} antisites.

The important question is the spatial distribution of native defects in the annealed samples. The concentration of In_{Sb} antisites near the surface can be considerably larger in comparison with the bulk one due to several reasons. Obviously, the most simple reason is the evaporation of Sb atoms from the surface. Another possibility of the surface enrichment with native defects has been pointed out by Höglund *et al*. [9]. Using the density-functional theory, they showed that the higher concentration of defects at the surface can be related to a lower formation energy as compared to that of bulk defects. The increased concentration of negatively charged defects induces the band bending at the surface. Beside these reasons, the band bending can arise due to the Fermi pinning at the top of the valence band by the surface states related to In_{Sb} antisites. In any case, the band bending results in formation of an accumulation layer as well as suppression of minority carrier recombination. The appropriate model of photocon-ductivity in semiconductors with the surface band bending has been developed in [16]. The consequence of this is the observed increase in the photocurrent in the annealed samples of InSb.

4. Conclusions

The conductivity type conversion was observed in *n*-InSb subjected the furnace annealing at temperatures 300, 370 and 400 °C for 30 min. The samples with the unencapsulated surface were used for annealing. Vacancies generated due to evaporation and segregation of volatile component (Sb) are assumed to be unstable with respect to formation of In_{Sb} antsites, which are acceptors in InSb. Antisite defects are more easily generated at the surface, which results in the band bending and formation of an accumulation layer. It leads to suppression of recombination of minority carriers (electrons) at the surface and to increase of photoresponse in the annealed samples. The density of antisites has been estimated to be of the order of $(2...4) \cdot 10^{14}$ cm^{-3}.

Appendix

Early results of experimental and theoretical investigations of photoconductivity in InSb were summarized in a number of monographs [17-20]. Below, we will follow Smith [18]. The continuity equation for the optically generated minority carriers (holes) is expressed as

$$D\frac{d^2\delta p}{dx^2} - \frac{\delta p}{\tau_p} = \Re \exp(-\alpha x), \qquad (A1)$$

where

$$\Re = \eta \alpha I(1-R)/\hbar\omega. \qquad (A2)$$

Here, I is the light intensity, R_s – surface reflection coefficient, η – quantum efficiency, D – ambipolar diffusion coefficient. Other symbols have their usual meanings. The solution to equation (A1) for a thick sample ($d \gg L$) is given by

$$\delta p = A\exp(-x/L) - \frac{\tau_p \Re \exp(-\alpha x)}{L^2\alpha^2 - 1}, \qquad (A3)$$

where the constant A can be found from the boundary condition

$$D\frac{d\delta p}{dx} = s\delta p. \qquad (A4)$$

The concentration of excess holes is

$$\delta p = \frac{\Re\tau_p}{\alpha^2 L^2 - 1}\left[\frac{\alpha L^2 + s\tau_p}{L + s\tau_p} e^{-\frac{x}{L}} - e^{-\alpha x}\right]. \qquad (A5)$$

In the above equations, transport of excess carriers is governed by ambipolar diffusion and drift. Since in this case the condition $n \gg p$ is fulfilled, the ambipolar diffusion coefficient and mobility are defined by holes. The spectral dependences of the absorption coefficient is approximated by the expressions [20]

$$\alpha = 1.9\times 10^4\left(h\nu - E_g\right)^{1/2} + 800 \qquad (A6)$$

for $\lambda < \lambda_g$ and

$$\alpha_1 = 800\exp\left(\frac{h\nu - E_g}{kT}\right) \qquad (A7)$$

for $\lambda > \lambda_g$. An appropriate expression for the temperature dependence of the band gap is taken from [4]. The calculated photocurrent is shown in Fig. 3.

References

1. Marrakchi G., Joly J.F., Vincent F. et al. Characteristics of electron traps in rapid thermal annealed GaAs using a capping proximity technique. *Appl. Surf. Sci.* 1989. **36**. P. 564–571.
2. Jialu Liu, Tingqing Zhang, Rapid thermal annealing characteristics of Be implanted into InSb. *Appl. Surf. Sci.* 1998. **126**. P. 231–234.
3. Kreutz E.W., Rickus E. and Sotnik N. The effect of temperature on the stoichiometry of InSb(110) surfaces. *Surf. Technol.* 1980. **11**. P. 171–177.
4. htpp://www.ioffe.ru/SVA/NSM/semicond/.
5. Jin Y.J., Zhang D.H., Chen X.Z., Tang X.H. Sb antisite defects in InSb epilayers prepared by metalorganic chemical vapor deposition. *J. Crystal Growth*. 2011. **318**. P. 356–359.
6. Sen Gupta A., Naidu S.V., Roy R., and Sen P. Vacancy formation energy in InSb from positron trapping measurements. *Solid State Communs.* 1986. **58**, No. 3. P. 219–222.
7. Kendall D.L., Huggins R.A. Self-diffusion in indium antimonide. *J. Appl. Phys.* 1969. **40**. P. 2750–2759.
8. Morozov A.N., Abaeva T.V., Bublik V.T. Effect of In and Sb vacancies on temperature dependence of InSb lattice parameter at high temperatures. *Cryst. Res. Technol.* 1986. **21**. P. 613–617.
9. Höglund A., Castleton C.W.M., Göthelid M., Johansson B., and Mirbt S. Point defects on the (110) surfaces of InP, InAs, and InSb: A comparison with bulk. *Phys. Rev. B*. 2006. **74**. P. 075332.
10. Tahini H.A., Chroneos A., Murphy S.T., Schwingenschlögl U., and Grimes R.W. Vacancies and defect levels in III–V semiconductors. *J. Appl. Phys.* 2013. **114**, No. 6. P. 063517.
11. Chroneos A., Tahini H.A., Schwingenschlögl U., and Grimes R.W. Antisites in III-V semiconductors: Density functional theory calculations. *J. Appl. Phys.* 2014. **116**, No. 2. P. 023505.
12. Hong Ky Nguyen, Pavesi L., Araújo D., Ganière J.D., and Reinhart F.K. Thermal conversion of *n*-type GaAs:Si to *p*-type in excess arsenic vapor. *J. Appl. Phys.* 1991. **70**, No. 7. P. 3887.
13. Ohkubo N., Shishikura M., and Matsumoto S. Thermal conversion of semiinsulating GaAs in high-temperature annealing. *J. Appl. Phys.* 1993. **73**, No. 2. P. 615–618.
14. Weng Yumin, Zheng Qingping, Fan Zhineng, Zong Xiangfu, Thermal conversion of semi-insulating GaAs due to gallium vacancies and anti-structure disorder. *Chin. Phys. Lett.* 1992. **9**, No. 7. P. 375–378.
15. Farrow R.L., Chang R.K., Mroczkowski S., and Pollak F.H. Detection of excess crystalline As and Sb in III-V oxide interfaces by Raman scattering. *Appl. Phys. Lett.* 1977. **31**, No. 11. P. 768–770.
16. Bir G.L. Effect of surface recombination on photoconductivity of semiconductors. *Fizika Tverd. Tela.* 1959. **1**, No. 1. P. 67–76 (in Russian).
17. Moss T.S., Burrell G.J., Ellis B. *Semiconductor Opto-Electronics*. Butterworth, 1973.
18. Smith R.A. *Semiconductors*, Second edition. Cambridge University Press, 1978.
19. *Infrared Photon Detectors*. Ed. by A. Rogalski. SPIE Opt. Eng. Press, N.Y., 1995.
20. Dereniak E.L. and Boreman G.D. *Infrared Detectors and Systems*. New York, John Wiley & Sons, Inc., 1996. P. 90.